Progress In Electromagnetics Research C, Vol. 128, 61–71, 2023

Electromagnetic Diffraction by a Slotted Cylinder with the Fractional Boundary Condition

Kamil Karaçuha[1, *], Vasil Tabatadze[2, 3], Ömer F. Alperen[2], Ertuğrul Karaçuha[2], and Eldar Veliev[2, 4]

Abstract—This study investigates several substantial questions arising in the diffraction by circular surfaces with the fractional boundary condition, which is the generalization of Dirichlet and Neumann boundary conditions. The study analyses the electromagnetic E-polarized plane wave diffraction by a slotted circular cylinder with the fractional boundary condition. For the first time, the fractional boundary condition regarding circular geometries is employed in the literature. The resonance characteristics for different boundary conditions, angle of incidence, and aperture sizes are analyzed. The new resonances are observed when the surface is different from the perfect electric or magnetic conducting surface.

1. INTRODUCTION

Electromagnetic scattering by the object with edges plays a crucial role in electromagnetic theory since the scattering phenomena yield different physical outcomes such as high or low radiation levels in an unexpected observation angle. Therefore, depending on the requirements, such problems and their accurate or approximate solutions have a substantial role in many branches of the electromagnetic research community, such as antenna and microwave component designs, radar cross-section analysis, and inverse scattering [1, 2]. Besides, the solutions to such problems guide the numerical methods for verifications and comparison. Apart from the importance of electromagnetic scattering regarding geometry, different boundary conditions subject to the surface also provide different solutions to the same geometry. This is the fundamental aim of the present study, which generalizes the Dirichlet and Neumann boundary conditions for circular geometries and provides important outcomes of electromagnetic scattering when the boundary conditions which are called fractional boundary conditions become in an interval of Dirichlet and Neumann boundary conditions. Depending on the fractional order, the boundary condition on the surface ranges from Dirichlet to the Neumann boundary condition. This is the first study regarding circular geometries subjecting to fractional boundary conditions. The reason that such problems have not been solved yet is that the fractional derivative of the Hankel function concerning the argument in a compact form has not been provided in the literature. Since the exponential function has a straightforward expression for the fractional derivative, the spectral representation of the Hankel function is employed while taking the fractional derivative of the corresponding function. Due to this, such an approach is very suitable for flat geometries like strips, half-plane, or wedges. However, it is preferred that the Hankel function is expanded as the summation of the Bessel and Hankel function by addition theorem [3] while having circular geometries or radial periodicity in general [4]. In the literature, a circular cylinder with a slotted slit has been intensively

Received 7 September 2022, Accepted 20 December 2022, Scheduled 29 December 2022

* Corresponding author: Kamil Karaçuha (karacuha17@itu.edu.tr).

[1] Electrical Engineering Department of Istanbul Technical University, Istanbul, Turky. [2] Informatics Institute of Istanbul Technical University, Istanbul, Turky. [3] Tbilisi State University, Tbilisi, Georgia. [4] National Technical University 'Kharkiv Polytechnic Institute', Kharkiv, Ukraine.

studied in the case of perfectly conducting surfaces and different polarization cases [5, 6]. However, few studies were conducted when the boundary condition differed from Dirichlet and/or Neumann boundary conditions [7–9]. In these studies, the impedance boundary condition is employed. For [7], the surface is resistive, and [8] is valid for only a high-frequency regime.

On the other hand, the present study enables us to generalize the boundary condition on such geometries and reveals critical new outcomes to the literature. In our previous studies, it was shown that there is a relation between the fractional order and the impedance value. The advantage of the proposed approach is that instead of considering electric and magnetic current densities on the scatterer's surface while solving the diffraction problem by the impedance surface, the fractional approach needs only one current density distribution, and the mathematical theory becomes simpler. In the case of the circular geometries, the mathematical theory is still simpler. The results again reveal a transition between PEC and PMC which means that the surface satisfying the fraction boundary condition again describes intermediate states. The analyses are done on the near- and far-fields, total radar cross-sections (TRCS), and resonances. The results are verified with previous studies and analytical outcomes in limiting cases. Previously, the fractional boundary condition in electromagnetics was employed in strip, half-plane, wedge, and double-strip problems [10–12]. In these problems, higher resonance values and intermediate resonance characteristics between perfect electric and magnetic conductor surfaces are observed between the fractional-order 0 and 1 (between Dirichlet and Neumann boundary conditions, respectively).

After the introduction, the study continues with the formulation of the problem where the mathematical background, field, and current expressions are derived. Then, the numerical result part investigates the calculated field expressions, TRCS, and resonances. After that, the conclusion is drawn.

2. FORMULATION OF THE PROBLEM

This section provides the mathematical background of electromagnetic scattering by a circular slotted strip with the fractional boundary condition. Apart from the previous scattering problems with the fractional boundary condition, the Fourier Series are employed due to periodicity in the ϕ direction instead of the Fourier transform in the case of the strip, double-strips, and half-plane problem [10, 13]. In Figure 1, the geometry of the problem is provided. As seen in Figure 1, the cylindrical strip has a radius a and an aperture size of $2(\pi-\theta)$. In the figure, (ρ, ϕ) stand for the cylindrical coordinate variables regarding the radial and angular directions for the observer, whereas $(\rho'=a, \phi')$ correspond to the same parameters at the source point, respectively.

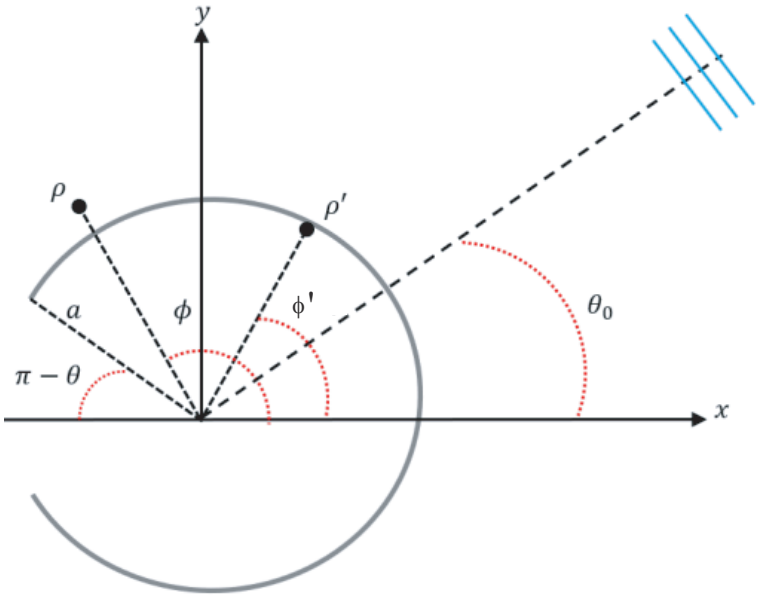

Figure 1. The geometry of the problem.

Before starting the details, it is better to summarize how to obtain the final expression. For simplicity, the fractional Green's function in two-dimensional space is expanded as the infinite summation of the Bessel and Hankel functions to split the arguments into two parts. The first main aim is to express the field components such as incident ($\vec{E}_z^0$) and scattered field ($\vec{E}_z^s$) in a mathematical form. Then, the fractional boundary condition is satisfied to obtain a system of linear algebraic equations (SLAE). To solve this SLAE, an analytical-numerical approach called orthogonal polynomials (OP) is preferred [14]. Then, the fractional boundary condition (FBC) is given in (1), where the total tangential electric field (E_z=E_z^0+E_z^s) is subject to the boundary condition on the surface [10]:

$$D_{k\rho}^{\nu}\, E_z\left(\rho,\phi\right)\big|_{\rho\to a\pm 0}=0, \quad \nu\in(0,1), \quad \phi\in[-\pi+\theta,\pi-\theta] \tag{1}$$

where $D_{k\rho}^{\nu}$ corresponds to the fractional derivative in the order of ν and with respect to $k\rho$. Here, k stands for the wavenumber, and ρ is the radial component. Note that the fractional order (FO) determines the surface characteristics. When FO becomes zero, the surface corresponds to PEC, whereas FO is equal to one case and stands for the PMC in the case of an E-polarized plane wave. As the fractional derivative of a function $f(x)$, the Riemann-Louivelle definition provided below is employed [15]:

$$D_x^{\nu} f\left(x\right)=\frac{1}{\Gamma\left(1-\nu\right)}\frac{d}{dx}\int_{-\infty}^{x}\frac{f\left(t\right)}{\left(x-t\right)^{\nu}}dt, \tag{2}$$

where $\Gamma(1-\alpha)$ is the Gamma Function and $\nu\epsilon(0,1)$.

To satisfy FBC in (1), the field components should be expressed in a mathematical form. In (3), the incident electric field is provided:

$$\vec{E}_z^0=e^{-ik\left(\alpha_0 x+\sqrt{1-\alpha_0^2}y\right)}\hat{e}_z=\sum_{m=-\infty}^{\infty} i^m J_m\left(k\rho\right)e^{im(\phi-\theta_0)}\hat{e}_z \tag{3}$$

Here, θ_0 is the incident angle; $\alpha_0=\cos\theta_0$; $k=2\pi/\lambda$; λ is the wavelength in free space; $\hat{e}_z$ is the unit vector along the z-axis; and J_n is the Bessel function. Besides, the time dependency is $e^{-i\omega t}$ and omitted throughout the study. It should be denoted that ω is the angular frequency. After expressing the incident wave in mathematical form, the scattered field is expressed as the convolution of the current density and the fractional Green's function (G^{ν}) [16, 17]:

$$E_z^s=\int_0^{2\pi}\mu\left(\phi'\right)G^{\nu}\left(k\left|\rho-\rho'\right|\right)d\phi', \tag{4}$$

$$\text{where} \qquad G^{\nu}\left(k|\rho-\rho'|\right)=i\frac{1}{4\pi}D_{k\rho}^{\nu}\left[H_0^{(1)}\left(k\left|\rho-\rho'\right|\right)\right]$$

Here, $\mu(\phi')$ is the current density of the obstacle, and $H_0^{(1)}$ is the Hankel function of the first kind and the zero-order. Note that $\mu(\phi')$ can have only non-zero values on the surface of the arc ($-\pi+\theta\leq\phi'\leq\pi-\theta$) because current may exist on the scatterer surface only.

The compact form of the fractional derivative of the Hankel function is not available in the literature. Therefore, the following references are employed to obtain the expression. $D_t^{\nu}H_0^{(1)}$ stands for the derivative of the Hankel function with respect to variable t in the order of ν, and the derivative of the Hankel function can be found as (5) [15, 18]. The details are attached in the Appendix.

$$\begin{aligned} D_t^{\nu}H_n^{(1)}\left(t\right) \;=\; & \frac{\left(t-\nu\right)^{-\nu}}{\Gamma\left(1-\nu\right)}H_n^{(1)}\left(t\right)+\sum_{p=1}^{\infty}\frac{\Gamma\left(\nu+1\right)}{\Gamma\left(p+1\right)\Gamma\left(\nu-p+1\right)}\frac{\left(t-\nu\right)^{p-\nu}}{\Gamma\left(p-\nu+1\right)} \\ & \times\left(\frac{1}{2}\right)^{p}\sum_{l=0}^{p}\left(-1\right)^{l}\frac{\Gamma(p+1)}{\Gamma(l+1)\Gamma(p-l+1)}H_{n+2l-p}^{(1)}(t) \end{aligned} \tag{5}$$

Since the current density is periodic regarding ϕ' variable, the current density can be expanded as the Fourier series as provided in (6). This is a very crucial point of the present study.

$$\mu\left(\phi'\right)=\frac{2i}{\pi\varepsilon}\sum_{m=-\infty}^{\infty}\mu_m e^{im\phi'}=\sum_{m=-\infty}^{\infty}\hat{\mu}_m e^{im\phi'} \tag{6}$$

where:

$$\hat{\mu}_m=\frac{1}{2\pi}\int_{-\pi+\theta}^{\pi-\theta}\mu\left(\varphi\right)e^{-im\phi'}d\phi'$$

Here, μ_m and $\hat{\mu}_m$ are the unknown constant coefficients.

Then, the addition theorem for the Hankel function is provided in (7) since the argument (ρ-ρ') in Green's function becomes decoupled which allows to apply boundary conditions and take derivative easier [3]. After this point, all definitions given above would be employed in manipulations. Then, the scattered electric field can be obtained as (8) by using (4), (6), and (7).

$$H_0^{(1)}\left(k\left|\rho-a\right|\right)=\begin{cases}\displaystyle\sum_{n=-\infty}^{\infty}J_n\left(k\rho\right)H_n^{(1)}\left(ka\right)e^{in(\phi-\phi')}, & \rho\leq a\\ \displaystyle\sum_{n=-\infty}^{\infty}J_n\left(ka\right)H_n^{(1)}\left(k\rho\right)e^{in(\phi-\phi')}, & \rho\geq a\end{cases} \tag{7}$$

$$E_z^s=\frac{4i}{\varepsilon}\sum_{m=-\infty}^{\infty}\mu_m\left.D_{k\rho}^{\nu}\right|_{\rho=a}\begin{cases}\displaystyle\sum_{n=-\infty}^{\infty}J_n\left(k\rho\right)H_n^{(1)}\left(ka\right)e^{in\phi}\delta_{mn}, & \rho<a\\ \displaystyle\sum_{n=-\infty}^{\infty}J_n\left(ka\right)H_n^{(1)}\left(k\rho\right)e^{in\phi}\delta_{mn}, & \rho>a\end{cases} \tag{8}$$

where

$$\delta_{mn}=\frac{1}{2\pi}\int_{0}^{2\pi}e^{i(m-n)\phi'}d\phi',\quad \rho'=a.$$

It should be highlighted that δ_{mn} is a Kronecker delta and yields non-zero value (equal to 1) only for m=n. Therefore, one summation is dropped, and the following simple expression for the scattered field is obtained. After expressing all-field components in a compact and suitable mathematical form, the boundary condition is applied to the total tangential component of the electric field on the surface (ρ=$a\pm 0$ and $\phi\in[-\pi+\theta,\pi-\theta]$) by inserting (3) and (9) into (1). Here, the derivative acts on $k\rho$ argument as seen in (9). With the addition theorem, only one term is affected for each region (ρ<a or ρ>a) by the fractional derivative in fractional Green's function.

$$E_z^s=\frac{4i}{\varepsilon}\sum_{m=-\infty}^{\infty}\mu_m\begin{cases}\left.D_{k\rho}^{\nu}\right|_{\rho=a}J_m\left(k\rho\right)H_m^{(1)}\left(\varepsilon\right)e^{im\phi}, & \rho<a\\ J_m\left(\varepsilon\right)\left.D_{k\rho}^{\nu}\right|_{\rho=a}H_n^{(1)}\left(k\rho\right)e^{im\phi}, & \rho>a\end{cases} \tag{9}$$

Here, ε=ka.

After satisfying the boundary condition, (10) is obtained.

$$2\pi\sum_{m=-\infty}^{\infty}\hat{\mu}_m\gamma_m e^{im\theta\eta}=-\sum_{m=-\infty}^{\infty}i^m D_{k\rho}^{\nu}J_m\left(\varepsilon\right)e^{im(\theta\eta-\theta_0)} \tag{10}$$

Here, γ_m=$D_{k\rho}^{\nu}J_m(\varepsilon)D_{k\rho}^{\nu}H_n^{(1)}(\varepsilon)$ and η=$\frac{\phi'}{\pi-\theta}$.

It should be noted that $D_{k\rho}^{\nu}|_{\rho=a}J_m(k\rho)$ would be denoted as $D_{k\rho}^{\nu}J_m(\varepsilon)$ or $J_m^{\nu}(\varepsilon)$ after this point. The change of variable $=\frac{\phi'}{\pi-\theta}$ is done to normalize the angle interval of the current density between -1

and 1. It should be highlighted that the current density function has only non-zero values in $[-1,1]$ by the corresponding change of variable since the current density would be expressed in orthogonal polynomials. One of the main aims of the study is achieved at this point. The goal is to obtain the SLAE by applying the FBC. Now, the question arises of how to solve the corresponding SLAE. An analytical-numerical approach is employed to obtain the solution where the induced current density on the scattered is expressed in orthogonal polynomials. In this geometry, Gegenbauer polynomials ($C_n^{\nu+\frac{1}{2}}$) are used as they are orthogonal in the interval $[-1,1]$, and it has a suitable weighting function for employing the orthogonal conditions. Then, the current density is expressed as:

$$\mu(\eta) = \left(1-\eta^2\right)^{\nu} \sum_{n=0}^{\infty} x_n C_n^{\nu+\frac{1}{2}}(\eta) \tag{11}$$

where x_n is the unknown constant coefficients and $\hat{\mu}_m = \frac{\theta}{2\pi} \int_{-1}^{1} \mu(\eta) e^{-im\theta\eta} d\eta$.

It should be noted that the current density should satisfy the edge condition regarding the surface characteristics. For $\nu = 0$ (PEC) case, at the edge, the current needs to diverge, whereas the current density at the edge should vanishes and converges to the zero for $\nu = 1$ (PMC) case. The weighting function $(1-\eta^2)^{\nu-\frac{1}{2}}$ satisfies this condition for the E-polarized diffraction problems for $\nu = 0$, $\nu = 1$, and intermediate cases [19, 20]. Then, $\hat{\mu}_m$ can be found as (12) [21, 22]:

$$\hat{\mu}_m = \frac{\theta}{\Gamma\left(\nu+\frac{1}{2}\right)} \sum_{n=0}^{\infty} (-i)^n x_n \beta_n^{\nu+\frac{1}{2}} \frac{J_{\nu+n+\frac{1}{2}}(m\theta)}{(2m\theta)^{\left(\nu+\frac{1}{2}\right)}} \tag{12}$$

Here,

$$\beta_n^{\nu+\frac{1}{2}} = \frac{\Gamma(2\nu+1+n)}{\Gamma(n+1)}$$

Finally, inserting (12) into (10) and employing the following properties given in (13) would provide the final version of the SLAE for faster converging numerical analysis as (14) [23, 24].

$$e^{im\theta\eta} = 2\left(\frac{2}{m\theta}\right)^{\nu+\frac{1}{2}} \Gamma(\nu+\frac{1}{2}) \sum_{k=0}^{\infty} i^k \left(k+\nu+\frac{1}{2}\right) J_{k+\nu+\frac{1}{2}}(m\theta)\, C_k^{\nu+\frac{1}{2}}(\eta) \tag{13}$$

$$2\pi\theta \sum_{p=0}^{\infty} (-i)^p x_p \beta_p^{\nu+\frac{1}{2}} Q_{pk}^{\nu+\frac{1}{2}} = A_k^{\nu+\frac{1}{2}} \tag{14}$$

where:

$$Q_{pk}^{\nu+\frac{1}{2}} = \sum_{m=-\infty}^{\infty} \gamma_m J_{\nu+p+\frac{1}{2}}(m\theta)\, J_{k+\nu+\frac{1}{2}}(m\theta) \left(\frac{1}{m\theta}\right)^{2\nu+1},$$

$$A_k^{\nu+\frac{1}{2}} = -\Gamma\left(\nu+\frac{1}{2}\right) 2^{\nu+\frac{1}{2}} \sum_{m=-\infty}^{\infty} i^m D_{k\rho}^{\nu} J_m(\varepsilon)\, e^{-im\theta_0} J_{k+\nu+\frac{1}{2}}(m\theta) \left(\frac{1}{m\theta}\right)^{\nu+\frac{1}{2}}$$

For details, the reader can go through [20, 25, 26].

To obtain the radiation pattern, the observation is done in the far zone ($k\rho \to \infty$). For the far-field approach, the radial and angular parts can be separated by using the asymptotic expressions of the Hankel function. Then, the scattered field is expressed as [17]:

$$E_z^s(x,y) = R(k\rho)\, \Phi(\phi) \tag{15}$$

Here,

$$R(k\rho) = \sqrt{\frac{2}{\pi k\rho}} e^{ik\rho - \frac{i\pi}{4}}, \Phi(\phi,\theta_0) = \sum_{m=-\infty}^{\infty} \sum_{p=0}^{\infty} Z_p A_{pm}(\varepsilon,\nu) e^{im\left(\phi-\frac{\pi}{2}\right)}$$

where:

$$A_{pm}(\varepsilon,\nu)=\frac{\pi\varepsilon\theta}{2i\Gamma(\nu)}J_m'(\varepsilon)\frac{J_{p+\nu}(m\theta)}{(2m\theta)^{\nu}},\quad Z_p=(-i)^p\sqrt{\beta}_p^{\nu}x_p,\quad \beta_\rho=\frac{\Gamma(2p+2v+1)}{\Gamma(p+1)}$$

Note that $R(k\rho)$ corresponds to the radial dependence of the scattered far-field expression whereas $\Phi(\phi)$ stands for the radiation pattern. To analyze the resonances, a total radar cross-section investigation is needed. To obtain TRCS, the following definition is considered:

$$\sigma_t=\frac{1}{(2\varepsilon)^2}\int_0^{2\pi}|\Phi|^2\,d\phi \tag{16}$$

Since the boundary condition is taken with respect to $k\rho$, extra terms are needed to compensate. Therefore, a balance is needed to normalize this increase. Without $(2\varepsilon)^2$ division (unitless parameter), the characteristics go up for higher wavelengths as expected. The reason that we are taking the derivative with respect to $k\rho$ in (1) is that $k\rho$ is a unitless parameter and does not change the unit of the electric field, but it brings an extra k term for the derivative since actually in the literature, the boundary condition is taken with respect to ρ not $k\rho$. This change is compensated by division.

3. NUMERICAL RESULTS AND COMPARISON

In this section, the numerical results obtained for the near-field distributions and TRCS are provided. The comparison is made with the analytical outcomes and the limit cases of the impedance surface on which the impedance value covers the PEC and PMC surface impedance at the limit [20, 26]. In Figure 2, the TRCS for different fractional orders is provided. The PEC case is compared with $\nu = 0$ case, and also PMC case is compared with $\nu = 1$ case. The comparison is done by a circular arc satisfying the impedance boundary condition where the limit cases are utilized to obtain PEC and PMC surfaces. As the corresponding figure shows, the results coincide with $\nu = 0$ and $\nu = 1$ with PEC and PMC, respectively. As it is noticed, the highest value in the first resonance is observed when the fractional order is 0.75.

In Figure 3, again, the TRCS is proved for different fractional orders to converge the resonance values obtained with the analytical outcomes. Note that the values should be close to the zeros of Bessel's

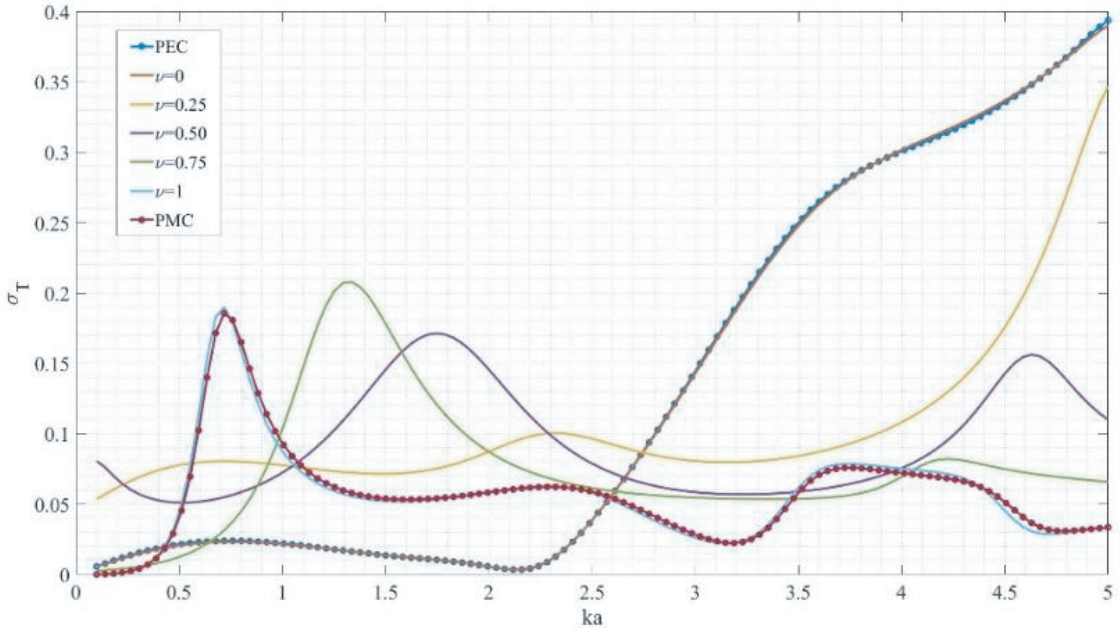

Figure 2. TRCS for $\theta_0 = \pi$, $\theta = \pi - \frac{\pi}{3}$, $a = 1$ meter.

function and its derivative regarding the boundary conditions (Dirichlet and Neumann, respectively) since for closed cylinders, resonances are observed at zeros of Bessel's function or zeros of the derivative of the Bessel's function. In our case, the cylinder is not closed, but it has a non-zero aperture. The

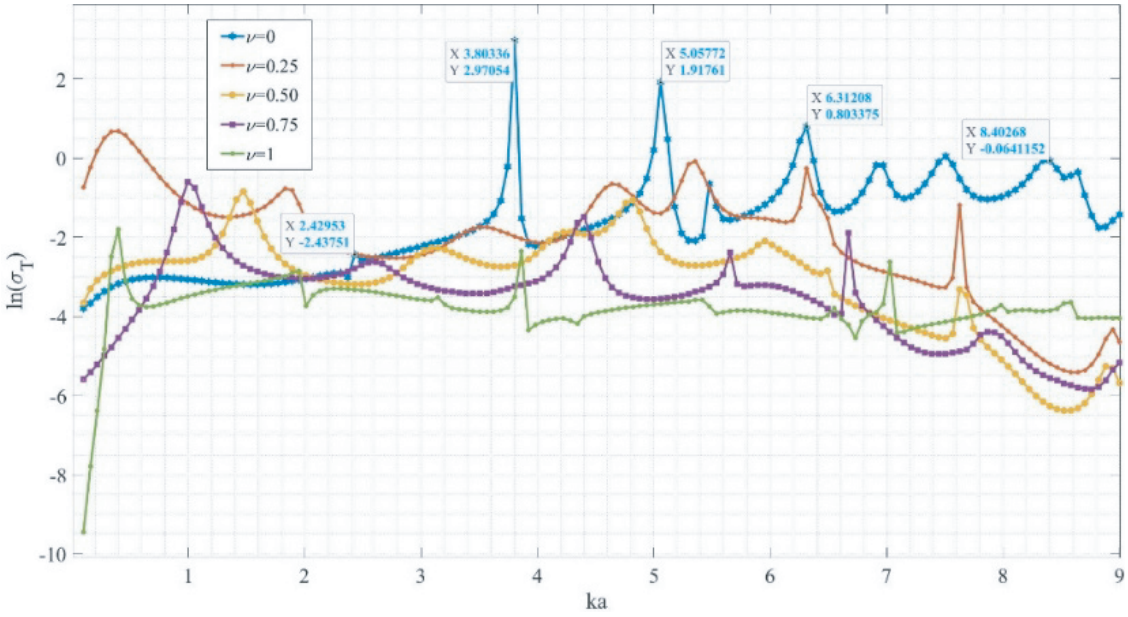

Figure 3. TRCS for $\theta_0 = \pi$, $\theta = \pi - \frac{\pi}{20}$, $a = 1$ meter.

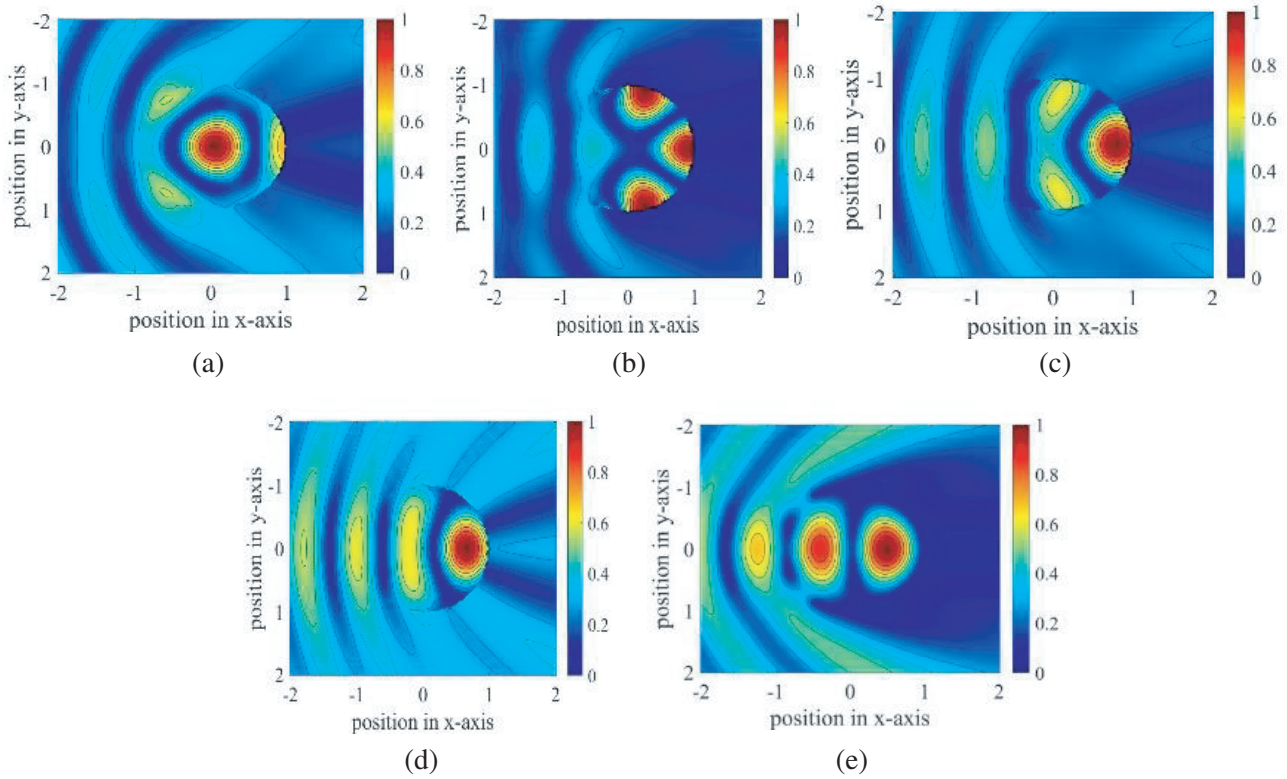

Figure 4. The normalized near electric field distributions ($\theta_o = \pi$, $\theta = \pi - \frac{\pi}{3}ka = 4$) for (a) $\nu = 1$, (b) $\nu = 0.75$, (c) $\nu = 0.5$, (d) $\nu = 0.25$, (e) $\nu = 0$.

natural logarithm of TRCS is taken for this figure to distinguish the resonances. As it is noticed, the resonances are approaching zeros of the Bessel function and its derivative for PEC and PMC cases, respectively. In the case of smaller apertures, the values are approaching the exact values.

The following figures provide the normalized near-electric field distributions for different parameters and comparisons. Figure 4 is a very crucial set of figures. In this figure, the evolution of the field distribution is observed regarding the transition of the modes. The field characteristics differ when the parameters are kept constant, and only the fractional order is changed. As seen from the figure, for PMC and PEC cases ((a) and (e), respectively), the boundary condition is satisfied as expected. The boundary condition is satisfied on the surface. Numerical verification can be done by looking at the tangential components of the total electric field on the surface. In the case of the Dirichlet condition ($\nu = 0$), the total tangential field should have vanished on the surface where the derivative of the total tangential component of the E-field should be nullified when the Neumann boundary condition ($\nu = 1$) is satisfied. Between them, the intermediate states are provided. One of the main advantages of the boundary condition is observing the transitions of the different modes by changing the fractional order and obtaining the intermediate states or modes in electrodynamics.

Furthermore, the comparison is provided in Figure 5. The comparison is achieved between the fractional and impedance arcs. In Figures 5(a) and 5(c), the normalized impedances (ξ) are provided, and it is observed that the field distributions are similar [26]. The fractional boundary condition is related to impedance boundary conditions like in the case of flat strip case [10]. Figure 4 reveals the same phenomena for circular geometries. The exact formulation of the relation between the intermediate fractional orders and the impedance values for circular geometries has not been derived yet. However, we found some coincidences for the specific values of the fractional order and impedance values.

In Figure 6, the different near-field distributions are presented to clarify the fractional boundary

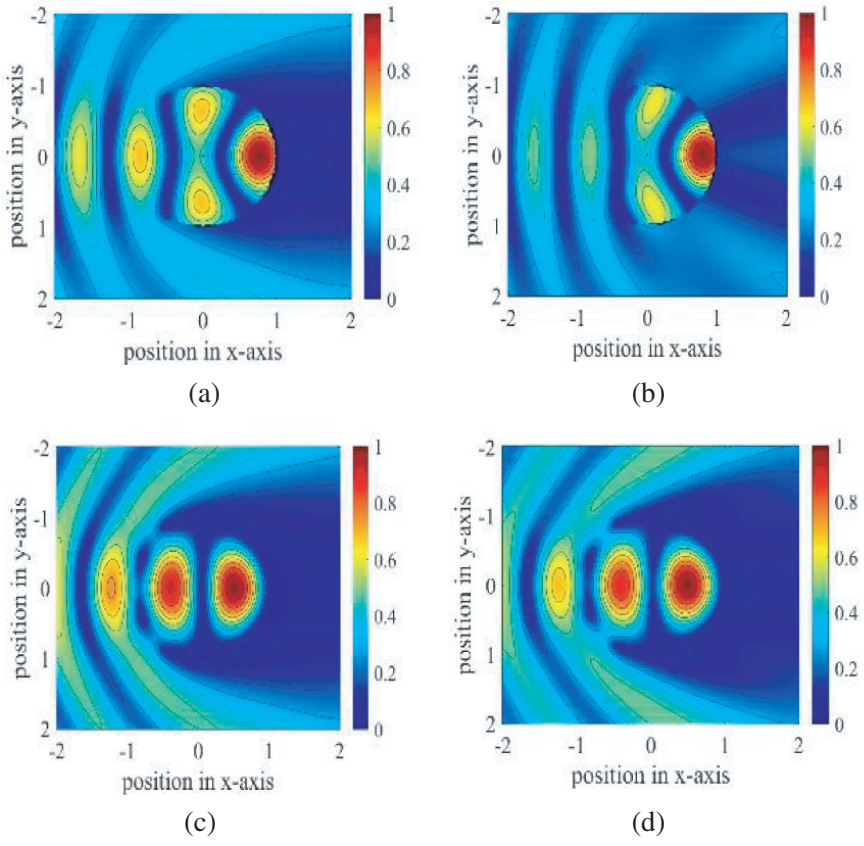

Figure 5. The normalized near electric field distributions ($\theta_o = \pi$, $\theta = \pi - \frac{\pi}{3}ka = 4$). (a) $\xi = 0.19i$. (b) $\nu = 0.52$. (c) $\xi = 10i$. (d) $\nu = 0$.

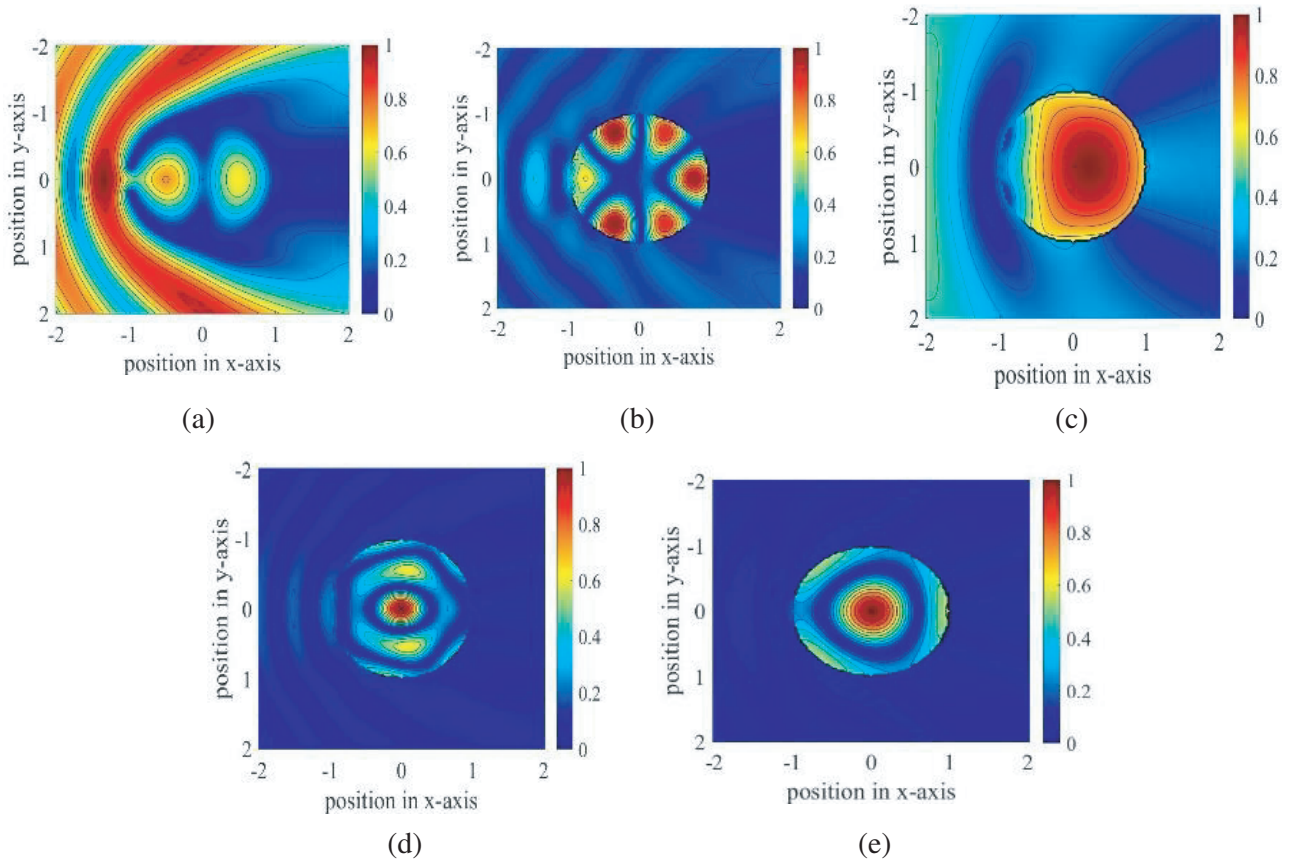

Figure 6. The normalized near electric field distributions ($\theta_o = \pi$, $\theta = \pi - \frac{\pi}{20}$, $a = 1$ meter). (a) $\nu = 0$, $k = 3.74$. (b) $\nu = 0.25$, $k = 5.35$. (c) $\nu = 0.5$, $k = 1.47$. (d) $\nu = 0.75$, $k = 6.67$. (e) $\nu = 0$, $k = 3.86$.

condition. Figure 6 shows several field distributions for resonance frequencies. We observe maximum peak values inside the arc in general. The incident angle is π.

In Figure 7, the oblique incident cases for different fractional orders are provided.

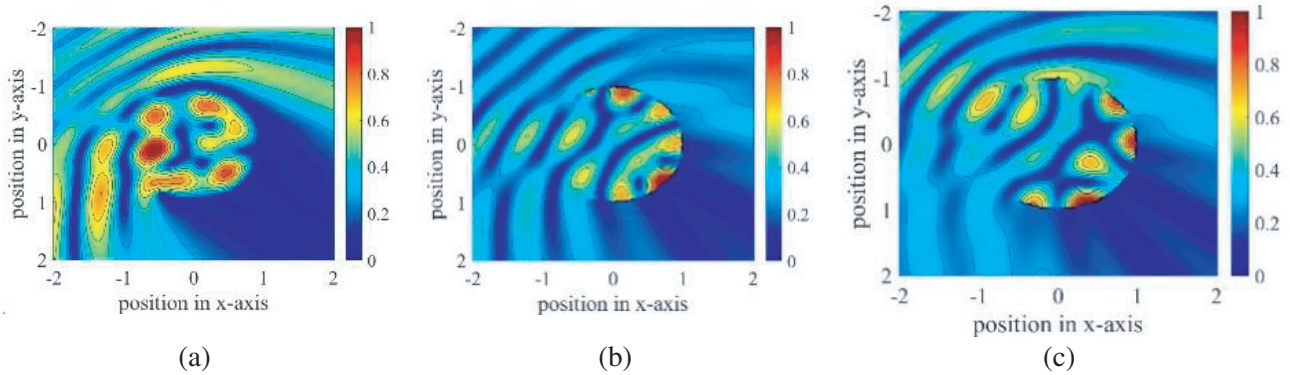

Figure 7. The normalized near electric field distributions ($\theta_o = \pi - \frac{\pi}{4}$, $\theta = \pi - \frac{\pi}{3}$, $ka = 2\pi$) for (a) $\nu = 0$, (b) $\nu = 0.5$, (c) $\nu = 1$.

4. CONCLUSION

The article discusses the solution to the electromagnetic diffraction problem for the circular arc with the fractional boundary condition. While changing the fractional order from 0 to 1, different electromagnetic behaviors for the arc are observed. Besides, resonant peaks become higher for specific values of the fractional order, different from 0 and 1. Also, it is noticed that the transition of the field modes between PEC and PMC fields, while changing the fractional order from 0 to 1, is validated. However, the mathematical relation between the impedance values and the fractional order for the circular geometries will be studied in the future. The comparison is made for PEC and PMC cases and one particular fractional order with the impedance arc. Here, new resonances are observed when the surface is different from the perfect electric or magnetic conducting surface. In other words, for the different fractional orders between 0 and 1, the resonant phenomena are observed and analyzed.

Furthermore, the results are compared with the analytical outcomes of zeros of the Bessel function and its derivative regarding the PEC and PMC cases, respectively. This is the first study regarding circular geometries with the fractional boundary condition. Thus, the new approach is followed in the case of the expression of Green's function and taking the fractional derivative of the Bessel and Hankel functions. The compact form of fractional derivative the Hankel function is proposed.

APPENDIX A.

The fractional derivative of a continuous function can be expressed as [15]:

$$D_t^{\alpha}\varphi\left(t\right)=\frac{\left(t-a\right)^{-\alpha}}{\Gamma(1-\alpha)}\varphi\left(t\right)+\sum_{k=1}^{\infty}\left(\begin{array}{c}\alpha\\k\end{array}\right)\frac{\left(t-a\right)^{k-\alpha}}{\Gamma\left(k-\alpha+1\right)}\varphi^{(k)}\left(t\right) \tag{A1}$$

where

$$\left(\begin{array}{c}\alpha\\k\end{array}\right)=\frac{\Gamma(\alpha+1)}{\Gamma(k+1)\Gamma(\alpha-k+1)}$$

For our problem, $\varphi(t)$ should be replaced by the Hankel function to obtain the fractional derivative of the Hankel function. However, the general derivative expression of the Hankel function is also needed, as seen on the right side of (A1). In (A2), the general expression of the integer derivative of the Hankel function is provided [18]:

$$\left(H_n^{(1)}(t)\right)^{(p)}=\left(\pm\frac{1}{2}\right)^p\sum_{l=0}^{p}\left(-1\right)^l\left(\begin{array}{c}p\\l\end{array}\right)H_{n\pm2l\mp p}^{(1)}(t) \tag{A2}$$

Then, the fractional derivative of the Hankel function is provided below:

$$\begin{aligned}D_t^{\alpha}H_n^{(1)}\left(t\right) \;=\; & \frac{\left(t-a\right)^{-\alpha}}{\Gamma\left(1-\alpha\right)}H_n^{(1)}\left(t\right)+\sum_{p=1}^{\infty}\frac{\Gamma(\alpha+1)}{\Gamma(p+1)\Gamma(\alpha-p+1)}\frac{\left(t-a\right)^{p-\alpha}}{\Gamma\left(p-\alpha+1\right)}\\ & \times\left(\frac{1}{2}\right)^p\sum_{l=0}^{p}\left(-1\right)^l\frac{\Gamma(p+1)}{\Gamma(l+1)\Gamma(p-l+1)}H_{n+2l-p}^{(1)}(t)\end{aligned} \tag{A3}$$

REFERENCES

1. Frezza, F., F. Mangini, and N. Tedeschi, "Introduction to electromagnetic scattering: Tutorial," *JOSA A*, Vol. 35, 163–173, 2018.
2. Bayvel, L. P., *Electromagnetic Scattering and Its Applications*, Springer Science & Business Media, 2012.
3. Balanis, C. A., *Advanced Engineering Electromagnetics*, John Wiley & Sons, 2012.
4. Vavilov, V. N., E. I. Veliev, V. V. Veremey, and V. P. Shestopalov, "Effective method of solution of diffraction problems for waves incident on a cylindrical screen," *Sov. Phys. Dokl.*, 640–644, 1990.

5. Beren, J., "Diffraction of an H-polarized electromagnetic wave by a circular cylinder with an infinite axial slot," *IEEE Trans. Antennas Propag.*, Vol. 31, 419–425, 1983.
6. Veliev, E. I. and V. P. Shestopalov, "Wave diffraction by intersecting circular cylindrical bodies," *Akad. Nauk SSSR Dokl.*, 1094–1098, 1985.
7. Nosich, A. I., Y. Okuno, and T. Shiraishi, "Scattering and absorption of E- and H-polarized plane waves by a circularly curved resistive strip," *Radio Sci.*, Vol. 31, 1733–1742, 1996.
8. Buyukaksoy, A. and G. Uzgoren, "Diffraction of high-frequency waves by a cylindrically curved surface with different face impedances," *IEEE Trans. Antennas Propag.*, Vol. 36, 690–695, 1988.
9. Umul, Y. Z., "Physical optics theory for the scattering of waves by an impedance strip," *Opt. Commun.*, Vol. 284, 1760–1765, 2011.
10. Veliev, E. I., T. M. Ahmedov, and M. V. Ivakhnychenko, "Fractional operators approach and fractional boundary conditions," *Electromagn. Waves*, 28, 2011.
11. Karaçuha, K., V. Tabatadze, and E. I. Veliyev, "Line source diffraction by double strips with different fractional boundary conditions," *Int. J. Appl. Electromagn. Mech.*, Vol. 67, 165–181, 2021.
12. Tabatadze, V., K. Karaçuha, and E. I. Veliyev, "The solution of the plane wave diffraction problem by two strips with different fractional boundary conditions," *Journal of Electromagnetic Waves and Applications*, Vol. 34, No. 7, 881–893, 2020.
13. Veliev, E., M. Ivakhnychenko, and T. Ahmedov, "Fractional boundary conditions in plane waves diffraction on a strip," *Progress In Electromagnetics Research*, Vol. 79, 443–462, 2008.
14. Karaçuha, K., "General approach to the line source electromagnetic scattering by a circular strip: Both E- and H-polarisation cases," *IET Microwaves, Antennas Propag.*, Vol. 15, 1721–1734, 2021.
15. Podlubny, I., "Fractional differential equations," *Math. Sci. Eng.*, Vol. 198, 41–119, 1999.
16. Veliev, E. I., A. I. Nosich, and V. P. Shestopalov, "Propagation of electromagnetic waves in a cylindrical waveguide with a longitudinal slit," *Radio Eng. Electron. Phys.*, Vol. 22, 466–473, 1977.
17. Karaçuha, K., V. Tabatadze, and E. I. Veliev, "Plane wave diffraction by strip with an integral boundary condition," *Turkish J. Electr. Eng. Comput. Sci.*, Vol. 28, 1776–1790, 2020.
18. Brychkov, Y. A., *Handbook of Special Functions: Derivatives, Integrals, Series and Other Formulas*, Chapman and Hall/CRC, 2008.
19. Meixner, J., "The behavior of electromagnetic fields at edges," *IEEE Trans. Antennas Propag.*, Vol. 20, 442–446, 1972.
20. Ikiz, T., S. Koshikawa, K. Kobayashi, E. I. Veliev, and A. H. Serbest, "Solution of the plane wave diffraction problem by an impedance strip using a numerical-analytical method: E-polarized case," *Journal of Electromagnetic Waves and Applications*, Vol. 15, No. 3, 315–340, 2001.
21. Tabatadze, V., K. Karacuha, and E. I. Veliyev, "The fractional derivative approach for the diffraction problems: Plane wave diffraction by two strips with the fractional boundary conditions," *Progress In Electromagnetics Research C*, Vol. 95, 251–264, 2019.
22. Karaçuha, K., V. Tabatadze, Ö. F. Alperen, and E. Veliev, "A new approach in electromagnetic plane wave diffraction by two concentric slotted cylinders with variably placed slits: E and H polarized cases," *IET Microwaves, Antennas Propag.*, Vol. 16, 437–450, 2022.
23. Prudnikov, A. P., I. A. Brychkov, and O. I. Marichev, *Integrals and Series: Special Functions*, CRC Press, 1986.
24. Vavilov, V. N., and E. I. Veliev, "Electromagnetic wave diffraction by cylindrical bodies with edges," *Electromagnetics*, Vol. 13, 339–357, 1993.
25. Karaçuha, K., V. Tabatadze, and E. I. Veliyev, "Electromagnetic plane wave diffraction by a cylindrical arc with edges: H-polarized case," *Int. J. Appl. Electromagn. Mech.*, 1–15, 2022.
26. Ivakhnychenko, M., E. Veliev, and T. Ahmedov, "Scattering properties of the strip with fractional boundary conditions and comparison with the impedance strip," *Progress In Electromagnetics Research C*, Vol. 2, 189–205, 2008.